UC Berkeley

UC Berkeley Previously Published Works

Title

The Nonmevalonate Pathway of Isoprenoid Biosynthesis Supports Anaerobic Growth of Listeria monocytogenes

Permalink

https://escholarship.org/uc/item/1bz75186

Journal

Infection and Immunity, 88(2)

ISSN

0019-9567

Authors

Lee, Eric D

Navas, Kathleen I

Portnoy, Daniel A

Publication Date

2020-01-22

DOI

10.1128/iai.00788-19

Peer reviewed

eScholarship.org Powered by the California Digital Library
University of California

AMERICAN SOCIETY FOR MICROBIOLOGY | Infection and Immunity®

CELLULAR MICROBIOLOGY:
PATHOGEN-HOST CELL MOLECULAR INTERACTIONS

The Nonmevalonate Pathway of Isoprenoid Biosynthesis Supports Anaerobic Growth of *Listeria monocytogenes*

Eric D. Lee,[a] Kathleen I. Navas,[b] Daniel A. Portnoy[b,c]

[a]Graduate Group in Infectious Diseases and Immunity, School of Public Health, University of California, Berkeley, Berkeley, California, USA
[b]Department of Molecular and Cell Biology, University of California, Berkeley, Berkeley, California, USA
[c]Department of Plant and Microbial Biology, University of California, Berkeley, Berkeley, California, USA

ABSTRACT Isoprenoids are an essential and diverse class of molecules, present in all forms of life, that are synthesized from an essential common precursor derived from either the mevalonate pathway or the nonmevalonate pathway. Most bacteria have one pathway or the other, but the Gram-positive, facultative intracellular pathogen *Listeria monocytogenes* is unusual because it carries all the genes for both pathways. While the mevalonate pathway has previously been reported to be essential, here we demonstrate that the nonmevalonate pathway can support growth of strains 10403S and EGD-e, but only anaerobically. *L. monocytogenes* lacking the gene *hmgR*, encoding the rate-limiting enzyme of the mevalonate pathway, had a doubling time of 4 h under anaerobic conditions, in contrast to the 45 min doubling time of the wild type. In contrast, deleting *hmgR* in two clinical isolates resulted in mutants that grew significantly faster, doubling in approximately 2 h anaerobically, although they still failed to grow under aerobic conditions without mevalonate. The difference in anaerobic growth rate was traced to three amino acid changes in the nonmevalonate pathway enzyme GcpE, and these changes were sufficient to increase the growth rate of 10403S to the rate observed in the clinical isolates. Despite an increased growth rate, virulence was still dependent on the mevalonate pathway in 10403S strains expressing the more active GcpE allele.

KEYWORDS bacteria, gamma delta T cells, mevalonate, virulence

Isoprenoids represent the largest family of compounds present in all living organisms and are used for a wide variety of processes, including cell wall synthesis, electron transport, and maintaining membrane fluidity (1). Isoprenoids are derived from the essential isoprenoid precursor molecules isopentenyl pyrophosphate (IPP) and dimethylallyl pyrophosphate (DMAPP). These precursors are synthesized by two distinct pathways, the mevalonate pathway and the nonmevalonate pathway (Fig. 1A). While mammals all use the mevalonate pathway (2), bacteria usually carry genes for only one of the two pathways (3). In rare instances bacteria lack both pathways, such as the obligate intracellular bacterium *Rickettsia parkeri*, but these bacteria depend on the host cell as a source for isoprenoid precursors (4). *Listeria monocytogenes* is a Gram-positive, facultative intracellular pathogen that, unlike most bacteria, has the genes for both the mevalonate and the nonmevalonate pathways (5). Work from others reported that the rate-limiting enzyme of the mevalonate pathway, HmgR, is essential in *L. monocytogenes* EGD-e, as strains lacking *hmgR* cannot grow unless supplemented with mevalonate in the growth media (6, 7). Deleting either of the last two enzymes in the nonmevalonate pathway, GcpE or LytB, had no impact on growth *in vitro* and a negligible effect on virulence (7).

While it is curious that *L. monocytogenes* has both isoprenoid precursor pathways, interest in these pathways also stems from observations that an intermediate molecule

Citation Lee ED, Navas KI, Portnoy DA. 2020. The nonmevalonate pathway of isoprenoid biosynthesis supports anaerobic growth of *Listeria monocytogenes*. Infect Immun 88:e00788-19. https://doi.org/10.1128/IAI.00788-19.

Editor Nancy E. Freitag, University of Illinois at Chicago

Copyright © 2020 American Society for Microbiology. All Rights Reserved.

Address correspondence to Daniel A. Portnoy, portnoy@berkeley.edu.

Received 3 October 2019
Returned for modification 15 November 2019
Accepted 21 November 2019
Accepted manuscript posted online 2 December 2019
Published 22 January 2020

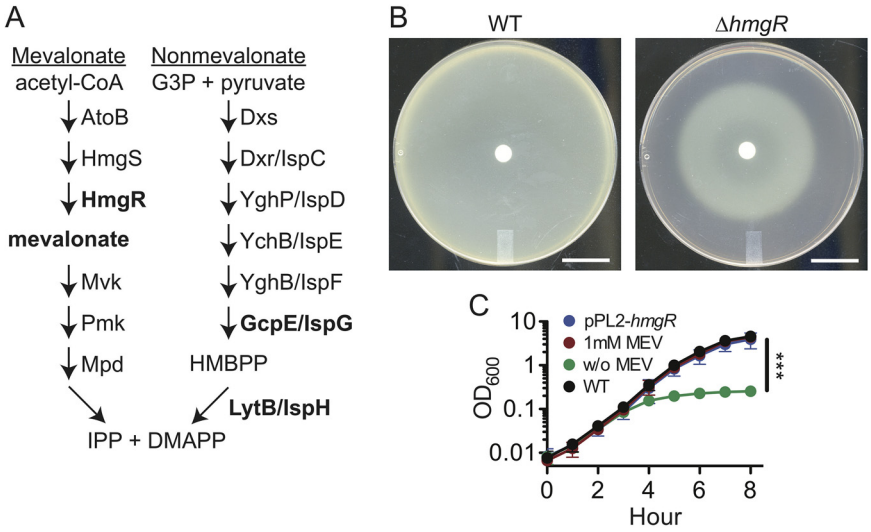

FIG 1 Mevalonate pathway is essential for aerobic growth. (A) Abbreviated diagram of *L. monocytogenes* isoprenoid precursor pathways. See reference 5 for the full pathway. (B) Disk diffusion assay using 10 μl of 1 M mevalonate on a BHI agar plate spread with the WT or 10403S Δ*hmgR* strain, demonstrating mevalonate-dependent growth. White bar is 20 mm. (C) Aerobic BHI growth curve of WT, 10403S Δ*hmgR* strain, and 10403S Δ*hmgR* strain with *hmgR* gene on the integrating plasmid pPL2. The 10403S Δ*hmgR* strain was grown in BHI supplemented with the indicated concentrations of mevalonate (MEV). ***, $P < 0.0001$.

of the nonmevalonate pathway, (E)-4-hydroxy-3-methyl-but-2-enyl pyrophosphate (HMBPP), activates Vγ9Vδ2 T cells, an innate-like T cell subset found in humans and nonhuman primates but not in mice (8). Upon activation by microorganisms with the nonmevalonate pathway or synthetic ligands, Vγ9Vδ2 T cells proliferate, produce proinflammatory cytokines, and have cytotoxic activity against cells presenting HMBPP (9). Vγ9Vδ2 T cells have a broad role communicating with innate and adaptive immune cells to coordinate responses to bacterial infections, but it has been difficult to gain a mechanistic understanding of their functions due to the challenge of developing an appropriate model system (10, 11).

L. monocytogenes is being developed as a cancer vaccine platform, using a live-attenuated recombinant bacterial strain to stimulate $CD8^+$ T cell responses (12). Despite impressive results in mice, human clinical trials have shown promising but limited responses to *L. monocytogenes*-based treatments. Given the potential role of Vγ9Vδ2 T cells in responses to HMBPP-producing *L. monocytogenes* in humans, we were interested in further understanding isoprenoid precursor pathways in strain 10403S, the bacterial strain used for these studies. Additionally, we were intrigued by the observation that *L. monocytogenes* contains both pathways, despite no reported function for the nonmevalonate pathway.

In this study, we further examined the role of the mevalonate and nonmevalonate pathways for *L. monocytogenes* growth and pathogenesis. Additionally, the nonmevalonate pathway was examined in two *L. monocytogenes* strains, FSL N1-017 (FSL), which was isolated from trout brine (13), and HPB2262 Aureli 1997 (HPB2262), which was isolated from an outbreak of gastroenteritis (14). These isolates were chosen because they are in *L. monocytogenes* lineage I, organisms which are far more prevalent in human listeriosis cases and are genetically distinct from 10403S and EGD-e, which are in lineage II (15). We found that the mevalonate pathway was not essential for growth when Δ*hmgR* mutants were cultured anaerobically, as strains with only the nonmevalonate pathway grew in the absence of mevalonate. Additionally, three amino acid differences found in the lineage I strains could significantly alter GcpE function in *L. monocytogenes* strain 10403S, resulting in improved anaerobic growth compared to that of wild-type (WT) *L. monocytogenes*. These results demonstrate that either the

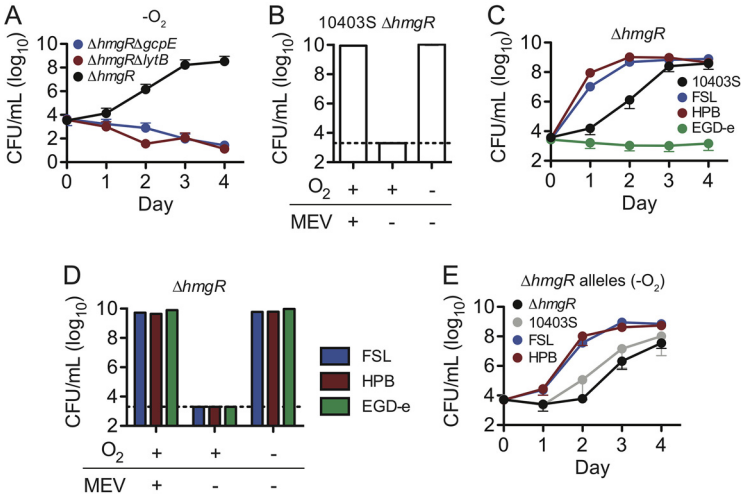

FIG 2 Nonmevalonate pathway is sufficient for anaerobic growth. (A) Anaerobic BHI growth curve of 10403S Δ*hmgR* strain compared to mutants in both pathways (10403S Δ*hmgR* Δ*gcpE* and 10403S Δ*hmgR* Δ*lytB* mutants). (B) Number of CFU measured after plating aerobic 10403S Δ*hmgR* cultures under indicated oxygen or mevalonate conditions. (C) Anaerobic growth of 10403S Δ*hmgR* compared to Δ*hmgR* mutants from indicated *L. monocytogenes* strains. (D) Number of CFU measured after plating aerobic FSL Δ*hmgR*, HPB Δ*hmgR*, and EGD-e Δ*hmgR* cultures under indicated oxygen or mevalonate conditions. (E) Anaerobic growth of 10403S Δ*hmgR* Δ*gcpE* strain with *gcpE* from indicated strains on pPL2 compared to that of 10403S Δ*hmgR* strains with *gcpE* on the chromosome.

mevalonate pathway or the nonmevalonate pathway is sufficient for *L. monocytogenes* growth under anaerobic conditions.

RESULTS

***L. monocytogenes* 10403S does not require the mevalonate pathway for anaerobic growth.** Consistent with previous reports (7), a 10403S strain lacking *hmgR* (the 10403S Δ*hmgR* strain) was unable to grow on brain heart infusion (BHI) agar unless supplemented with mevalonate (Fig. 1B). In liquid media the growth of 10403S Δ*hmgR* was fully restored with 1 mM mevalonate or if *hmgR* was complemented on an integrating plasmid, pPL2 (Fig. 1C).

The last two enzymes of the nonmevalonate pathway, GcpE and LytB, contain [4Fe-4S] iron-sulfur clusters (FeS clusters) (16, 17). In the presence of oxygen, FeS clusters can be oxidized, leaving a catalytically inactive $[3Fe\text{-}4S]^{1+}$ FeS cluster (18). GcpE and LytB (also referred to as IspG and IspH, respectively) are particularly oxygen labile in other organisms, since the FeS cluster is solvent exposed (19–21). We hypothesized that *L. monocytogenes* growth using the nonmevalonate pathway was promoted anaerobically due to decreased oxidation of GcpE or LytB FeS clusters. Indeed, strains lacking *hmgR* grew in the absence of mevalonate, although they exhibited a severe increase in doubling time, increasing from 43 min aerobically with mevalonate to approximately 4 h anaerobically without mevalonate (Fig. 2A). Additionally, the 10403S Δ*hmgR* strain formed a visible colony overnight on BHI agar supplemented with mevalonate, while it required 4 to 5 days to form similarly sized colonies anaerobically without mevalonate. Growth was dependent on the nonmevalonate pathway, as mutants in both pathways (10403S Δ*hmgR* Δ*gcpE* and 10403S Δ*hmgR* Δ*lytB* mutants) lost viability over the course of the anaerobic experiment (Fig. 2A) and did not form colonies on BHI agar anaerobically without mevalonate.

To examine whether anaerobic growth was a result of acquired suppressor mutations, the plating efficiency of strains was examined under aerobic and anaerobic conditions after overnight cultures were plated with or without mevalonate or oxygen. Aerobically, no 10403S Δ*hmgR* colonies grew unless the media contained mevalonate. Anaerobically, equal numbers of bacteria were recovered without mevalonate relative to media with mevalonate (Fig. 2B). Collectively, these data indicate that the nonmevalonate pathway supports growth in the absence of the mevalonate pathway.

Growth phenotype of mevalonate pathway mutants in other *L. monocytogenes* strains. Previous work on *L. monocytogenes* isoprenoid precursor pathways was conducted using strain EGD-e, where the mevalonate pathway was found to be essential (7). However, the authors did not examine anaerobic growth of their mevalonate pathway mutant, so we were curious whether any strain-specific growth differences existed between EGD-e and 10403S. The mevalonate pathway was deleted in EGD-e (EGD-e Δ*hmgR* strain) and two lineage I strains, *L. monocytogenes* FSL N1-017 (FSL Δ*hmgR* strain) and *L. monocytogenes* HPB2262 (HPB Δ*hmgR* strain). No growth defects were observed when the parental strains (EGD-e, FSL N1-017, and HPB2262) were cultured anaerobically or when Δ*hmgR* mutants were cultured with mevalonate, either aerobically or anaerobically (data not shown). Both lineage I strains doubled in approximately 2 h when *hmgR* was deleted, which was significantly faster than the 10403S Δ*hmgR* strain (Fig. 2C). The EGD-e Δ*hmgR* strain grew on BHI agar anaerobically without mevalonate (see Fig. S1 in the supplemental material) but did not grow in liquid culture, preventing the measurement of a doubling time. Additionally, when the plating efficiency of these strains was measured, equal numbers of bacteria were recovered anaerobically without mevalonate relative to media with mevalonate (Fig. 2D), similar to what was observed with the 10403S Δ*hmgR* strain.

To determine whether there was a genetically encoded basis for the observed differences in growth, we compared the 5′ untranslated regions (UTRs) and coding sequences of 10403S, FSL N1-017, and HPB2262 for each gene in the nonmevalonate pathway. Three genes, *dxr*, *ispE*, and *ispF*, were identical among all three strains. The 5′ UTR of *ispD* differed between strains, but no growth differences were observed when the genes for *ispD* or *lytB* from the lineage I strain were introduced into the 10403S Δ*hmgR* strain. However, strains complemented with *gcpE* from either FSL N1-017 or HPB2262 grew significantly faster than strains with 10403S *gcpE* (Fig. 2E).

Three residues in GcpE account for differences in anaerobic growth. GcpE chimeric proteins were constructed to more precisely identify the molecular origin of the growth differences between 10403S and the lineage I strains. First, the 5′ UTRs and coding sequences from each strain were exchanged and introduced into the 10403S Δ*hmgR* Δ*gcpE* strain. Only strains complemented with the protein-coding sequence from either lineage I strain grew significantly faster, even if expressed downstream of the 10403S 5′ UTR (Fig. 3A). Twelve amino acid differences exist in GcpE between 10403S and the lineage I strains. A chimeric protein was constructed containing the N-terminal portion of 10403S and the C-terminal portion of the FSL N1-017 protein, from amino acid 251 (Fig. 3B). The C-terminal end was chosen because it contained all four residues involved with FeS cluster coordination and the majority of the catalytic residues. Strains complemented with the chimeric strain grew as well as strains with the entire FSL N1-017 gene (Fig. 3C).

The C-terminal end of GcpE has nine differences between the lineage I strains and 10403S, the majority of which are located in three distinct areas; therefore, we focused on those changes. Two pairs of mutations, GcpE$^{I343V/D344E}$ and GcpE$^{F357Y/V359E}$, had no impact on anaerobic growth (Fig. 3D). Mutating three other residues in combination, GcpE$^{K291T/E293K/V294A}$ (GcpE*), significantly increased the growth rate of the 10403S Δ*hmgR* Δ*gcpE* strain, while the single mutants of either GcpE^{K291T} or GcpE^{V294A} were not sufficient to increase growth rate (Fig. 4A). Furthermore, when the same GcpE* mutations were made on the chromosome rather than on a plasmid, the resulting 10403S Δ*hmgR gcpE** strain had an anaerobic growth rate identical to that of the FSL Δ*hmgR* strain (Fig. 4B).

Given the distinct growth differences between the 10403S Δ*hmgR* and 10403S Δ*hmgR gcpE** strains, we sought to understand how these mutations impacted protein function. The protein structure prediction program Phyre2 was used to generate a model of GcpE based on the crystal structure from *Aquifex aeolicus* (strain VF5). The predicted structure placed residues 291 to 294 in a loop distal from both the FeS cluster and the catalytic TIM barrel in the protein (Fig. 4C), providing little insight into the mechanism by which these mutations alter 10403S Δ*hmgR gcpE** strain anaerobic growth.

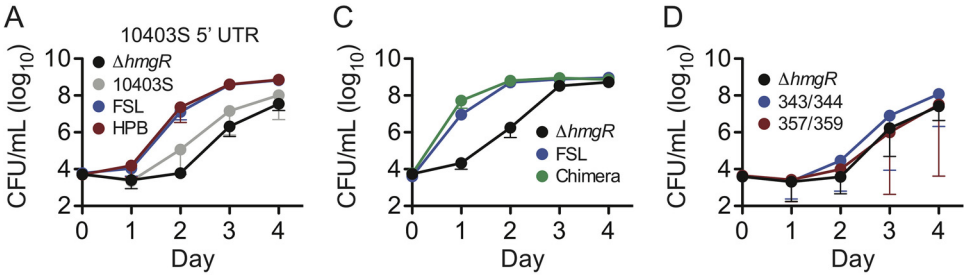

B

```
10403S       1 MNERIFRENTRPVQVGNLTIGGSEELTIQSMTTTKTHDVEATVAEIHRLEEAGCQIVRVACPDERAANALSAIKKKIHIP
EGD-e        1 ................................................................................
FSL N1-017   1 ........K.......................................V.......................R....
HPB2262      1 ........K.......................................V.......................R....

10403S      81 LVADIHFDYRLALKAIDAGVDKIRINPGNIGRRDRVEKVVNAAKAKNIPIRIGVNAGSLEKKIIQKYGYPTADGMVESAL
EGD-e       81 ................................................................................
FSL N1-017  81 ................................................................................E.......
HPB2262     81 ................................................................................E.......

10403S     161 AHIKILEDLDFYDIIVSLKASDVNLAIEAYDKASRAFNYPLHLGITESGTQFAGGIKSAAGLGAILSLGIGNTLRVSLSA
EGD-e      161 ................................................................................
FSL N1-017 161 ................................................................................
HPB2262    161 ................................................................................

10403S     241 DPVEEIKVAREVLKSFGFSSNAAMLISCPTCGRIEIDLIRIANEVENYIAKIEVPIKVAVLGCAVNGPGEAREADIGIAG
EGD-e      241 ................L...............................................................
FSL N1-017 241 ................L.............................T.KA.....................
HPB2262    241 ................L.............................T.KA.....................

10403S     321 SNGEGLLFRHGKIIRKVPEAIMIDELKKEIDILAEEFFVKKIDLESLR
EGD-e      321 ...................................................
FSL N1-017 321 ....................VE............Y.E..T......
HPB2262    321 ....................VE............Y.E..T......
```

FIG 3 Increased growth of lineage I strains is caused by changes in GcpE coding sequence. (A) Anaerobic growth of 10403S Δ*hmgR* Δ*gcpE* strain complemented with the *gcpE* coding sequence from different strains, all expressed from the 10403S 5′ UTR. (B) Sequence alignment of *L. monocytogenes* GcpE found in two lineage I strains and two laboratory strains. Listed residues indicate sequence differences relative to 10403S. (C) Anaerobic growth of 10403S Δ*hmgR* and FSL N1-017 Δ*hmgR* strains and 10403S Δ*hmgR* Δ*gcpE* strain complemented with a GcpE chimera containing the N-terminal domain (amino acids 1 to 250) from 10403S and the C-terminal domain from FSL N1-017 (amino acids 251 to 369). (D) Anaerobic growth of the 10403S Δ*hmgR* Δ*gcpE* strain complemented with point mutation GcpE$^{I343V/D344E}$ or GcpE$^{F357Y/V359E}$.

Nonmevalonate pathway function does not alter *L. monocytogenes* virulence in mice. Previous studies found minimal virulence defects when the nonmevalonate pathway was mutated in EGD-e (6, 7, 22), so we were curious whether 10403S had a similar phenotype. No significant virulence defects were observed in an intravenous (i.v.) infection (Fig. S2A) or a 5-day oral infection (Fig. S2B) with nonmevalonate pathway mutants. Furthermore, there were no differences in virulence between 10403S Δ*hmgR* and 10403S Δ*hmgR gcpE** strains in an i.v. infection (Fig. 5A) and oral infection (Fig. 5B) model, as both had significant virulence defects but were not different from each other.

We hypothesized that the nonmevalonate pathway makes a minor contribution to growth, and if so, differences may become apparent in a long-term oral infection model. During an oral infection, systemic bacterial dissemination adds an additional layer of complexity for understanding bacterial survival in the gut. Bacteria that spread from the gut can colonize the gallbladder and reseed the intestinal tract (23–25). This reservoir of bacteria is then the principal source of bacteria shed in the feces, rather than bacteria that have only survived in the anaerobic environment of the gut. Therefore, to prevent systemic dissemination and more closely examine long-term survival, a transposon (26) was used to disrupt the essential virulence factor listeriolysin O in our WT strain (10403S *hly*::Tn*917*), both nonmevalonate pathway deletions (10403S Δ*gcpE hly*::Tn*917* and 10403S Δ*lytB hly*::Tn*917*) and the fast-growing GcpE mutant (10403S *gcpE* hly*::Tn*917*). After oral infection, the number of *L. monocytogenes* CFU in the feces decreased over time, but mice continued to shed detectable amounts of bacteria 31 days postinfection (Fig. 5C). Previous studies show that mice

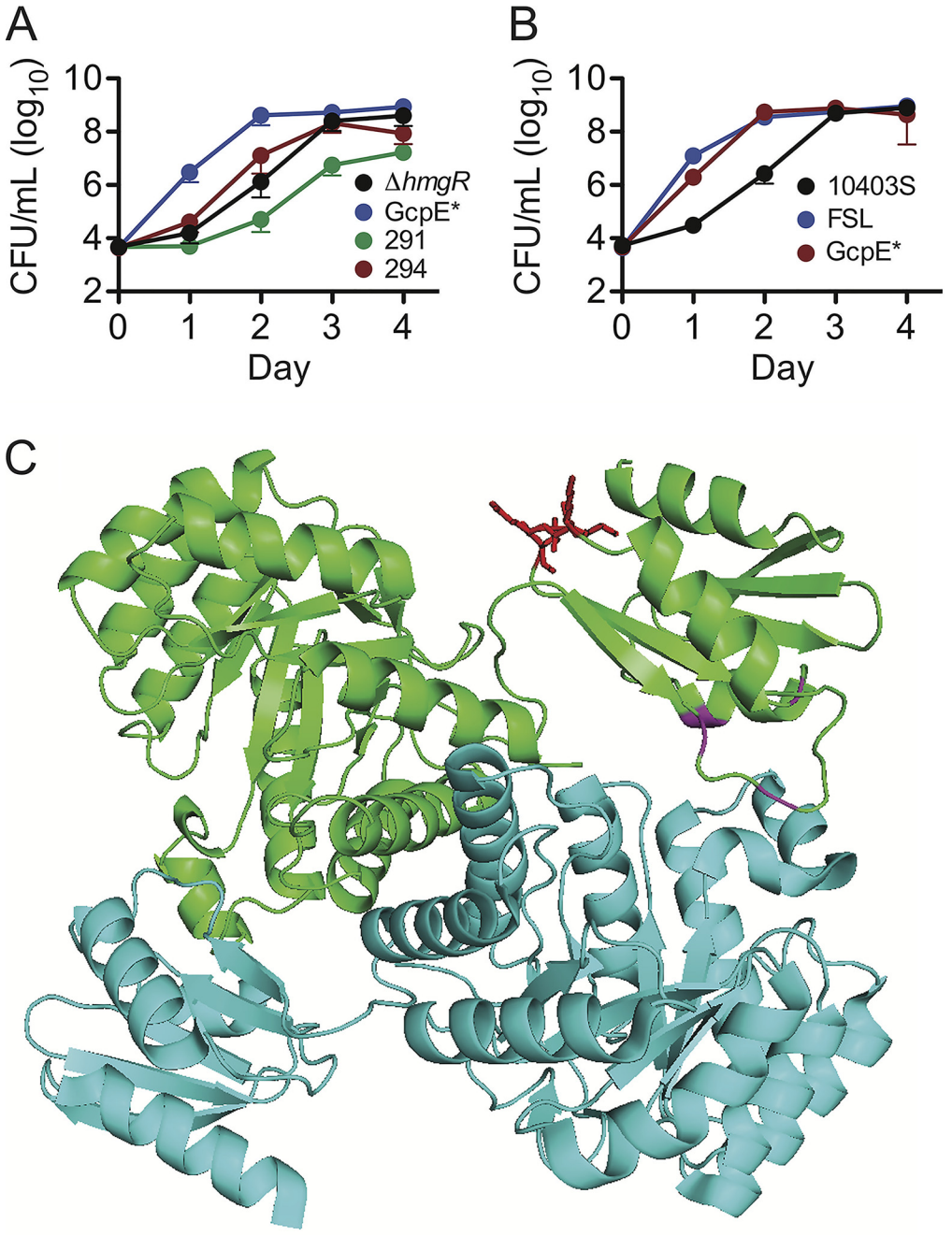

FIG 4 Point mutations fixing GcpE function increase anaerobic growth. (A) Anaerobic growth of Δ*hmgR* Δ*gcpE* strain complemented with GcpE$^{K291T/E293K/V294A}$ or point mutations GcpE^{K291T} and GcpE^{V294A}. (B) Anaerobic growth of 10403S Δ*hmgR* strain, FSL N1-017 Δ*hmgR* strain, and 10403S Δ*hmgR* strain with GcpE$^{K291T/E293K/V294A}$ mutation on the chromosome. (C) Predicted GcpE structure generated with Phyre2 protein structure prediction software. Two GcpE dimers, colored in green and cyan, with iron-sulfur cluster coordinating residues colored in purple and residues 291 to 294 colored in red.

stop shedding WT bacteria 2 weeks postinfection in a streptomycin pretreatment model (27), so it was unexpected that all 10403S *hly*::Tn*917* strains continued to be shed 4 weeks postinfection. While small differences in the median number of CFU shed from mice were noted, these changes did not rise to the level of statistical significance. These data suggest that the increased *in vitro* anaerobic growth with a GcpE* mutation does not impact bacterial survival when the bacteria are confined to the gut of mice.

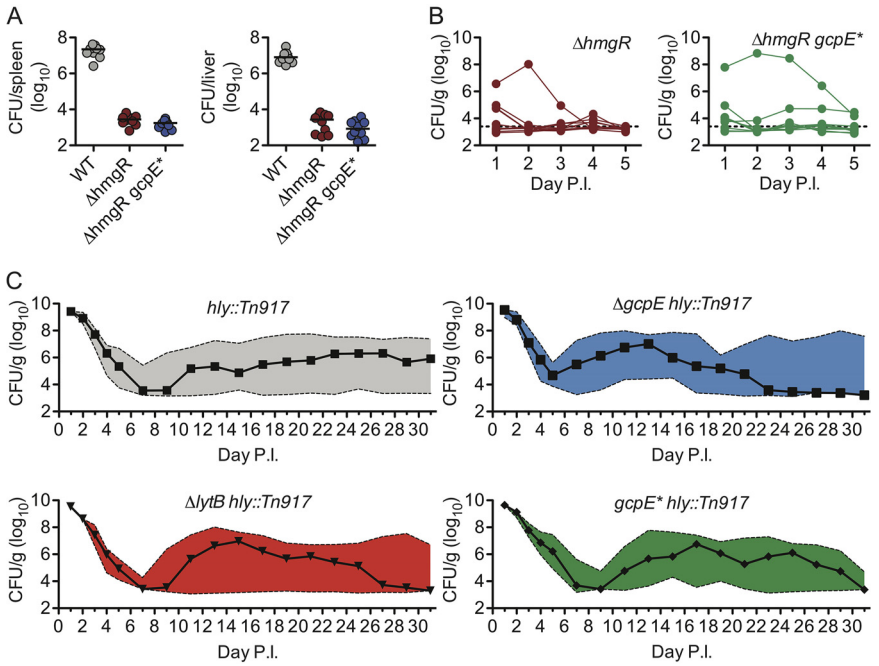

FIG 5 *L. monocytogenes* virulence in mice does not change with increased nonmevalonate pathway growth. (A) Number of CFU recovered from indicated organs 1 day after i.v. infection with indicated *L. monocytogenes* strains. Data show two independent experiments, with ten mice total for each strain, plotting medians and interquartile ranges. (B) Number of CFU recovered from mice 5 days after oral infection with indicated *L. monocytogenes* strains. Data show two independent experiments, with ten mice total for each strain. (C) Number of CFU recovered from pellets after oral infection with indicated *L. monocytogenes* strains. Plotted line is median number of CFU from two independent experiments (10403S *hly*::Tn*917*, 10403S *gcpE* hly*::Tn*917*, $n = 20$; 10403S Δ*gcpE*, 10403S Δ*lytB*, $n = 15$), and the shaded area is the interquartile range. P.I., postinfection.

DISCUSSION

The results of this study showed that the *L. monocytogenes* mevalonate pathway was essential for growth aerobically and supports growth anaerobically, while the nonmevalonate pathway was sufficient for growth only anaerobically. This growth phenotype was observed in four *L. monocytogenes* strains, although strains FSL N1-017 and HPB2262 lacking *hmgR* grew significantly faster than 10403S and EGD-e. Genetic approaches were used to identify three amino acid residues in the nonmevalonate pathway enzyme GcpE that were sufficient to eliminate differences in anaerobic growth between strains. A strain with GcpE$^{K291T/E293K/V294A}$ mutations grew more rapidly in pure culture but did not have significantly altered growth phenotypes in mice.

As a facultative anaerobe, *L. monocytogenes* substantially reprograms its metabolism in the absence of oxygen (28). We show that the nonmevalonate pathway functions anaerobically but note that *L. monocytogenes* still grows faster using the mevalonate pathway. This implies that there may be unidentified anaerobic growth conditions where the nonmevalonate pathway is required or beneficial for growth. Aerobically, *L. monocytogenes* uses oxygen as a terminal electron acceptor to maintain NAD^+/NADH ratios while pyruvate is converted to a variety of reduced (lactate and ethanol) and oxidized (acetate and acetoin) fermentation products. Anaerobically, pyruvate represents the primary electron acceptor, and consequently, the reduced fermentation product lactate predominates (29). Reflecting these metabolic changes, pyruvate dehydrogenase is downregulated anaerobically and, presumably, less acetyl coenzyme A (acetyl-CoA) is generated (28). The mevalonate and nonmevalonate pathways start with distinct molecules to generate isoprenoid precursors. The mevalonate pathway uses two molecules of acetyl-CoA, while the nonmevalonate pathway uses one molecule of pyruvate and one molecule of glyceraldehyde 3-phosphate. Under anaerobic condi-

tions, the metabolic shift toward lactate fermentation may limit acetyl-CoA levels, or the acetyl-CoA that is present may need to be used for NAD^+ regeneration. As a result, *L. monocytogenes* may use the nonmevalonate pathway anaerobically as an acetyl-CoA-independent means of producing isoprenoid precursors. However, under conditions used in this study, the mevalonate pathway was sufficient.

We hypothesize that the nonmevalonate pathway fails to function aerobically in *L. monocytogenes* because GcpE and LytB are oxygen-labile, FeS cluster-containing enzymes. FeS clusters are essential metal cofactors in enzymes but can be oxidized and lost in the presence of oxygen. As a result, organisms have developed mechanisms for protecting FeS clusters from oxidation, including multiple biosynthetic pathways to produce replacement FeS clusters for those damaged by oxidative stresses (30). Three distinct pathways for FeS cluster synthesis have been identified and designated the Nif, Suf, and Isc systems (31). The Gram-negative bacterium *Escherichia coli* has both the Isc and Suf systems (32, 33), while the Gram-positive model organism *Bacillus subtilis* and *L. monocytogenes* only have the Suf system. Isc and Suf genes are essential, but recent studies show that they are essential for synthesizing the FeS clusters in GcpE and LytB (34, 35). *B. subtilis* only encodes the nonmevalonate pathway but grows aerobically, which suggests that *L. monocytogenes* is fundamentally different from *B. subtilis* and may have a defect synthesizing FeS clusters, which prevents it from using the nonmevalonate pathway aerobically.

The crystal structure of *L. monocytogenes* GcpE has not been solved, but structures from other organisms point toward a mechanism by which mutations in GcpE may alter enzyme function (36–39). GcpE has two major domains, consisting of a catalytic TIM barrel at the N-terminal end and an FeS cluster coordinated by three cysteine residues and one glutamic acid residue at the C-terminal end. The protein forms a homodimer consisting of two subunits aligned head-to-tail. This allows the FeS cluster of one subunit to catalyze reactions in the active site of the opposite subunit, but this mechanism requires the C-terminal domain to rotate significantly while closing on a ligand (38, 40). We hypothesize that all three amino acid changes identified are necessary to alter enzyme kinetics and allow catalysis to proceed more quickly.

Dozens of preclinical studies and clinical trials have used *L. monocytogenes* 10403S as a vaccine vector for cancer immunotherapy (12, 41–45). All the strains used in these studies produce HMBPP based on the observation that they stimulate Vγ9Vδ2 T cells (43). Based on the results of this study, we predict that 10403S makes less HMBPP than the lineage I strains, although absolute HMBPP concentrations have not been directly measured. The role of Vγ9Vδ2 T cells is still unclear, so it is difficult to determine whether cellular activation in response to HMBPP enhances or diminishes the efficacy of an *L. monocytogenes*-based vaccine in primates. However, characterizing HMBPP production in the presence of the mevalonate pathway and metabolically engineering 10403S to produce more HMBPP may be useful to improve our understanding of Vγ9Vδ2 T cells and their role in vaccine development (46).

The two *L. monocytogenes* isolates used in this study raise interesting questions about the relationship between the nonmevalonate pathway and *L. monocytogenes* pathogenesis in humans. HPB2262 was isolated from an outbreak of febrile gastroenteritis caused by contaminated corn salad (14), but the symptoms of the outbreak were unique because the disease was almost exclusively noninvasive. In contrast, FSL N1-017 was isolated from trout in brine and is not associated with any human outbreaks. However, it is closely related to strain FSL R2-503, which is a clinical isolate from a different outbreak of gastroenteritis (13, 47). It is possible that having a functional nonmevalonate pathway provides *L. monocytogenes* strains with a selective growth advantage in the human gut. Alternatively, they may have a greater capacity to produce HMBPP and stimulate Vγ9Vδ2 T cells, which may trigger an immune response that contributes to disease (48). However, separating causative versus correlative factors related to Vγ9Vδ2 T cells would be challenging, given the absence of animal models and likelihood that other genes in lineage I *L. monocytogenes* strains influence pathogenesis.

TABLE 1 *L. monocytogenes* strains

Strain	Description	Reference or source
DP-L6253	10403S WT	59
DP-L6700	Δ*hmgR*	This study
DP-L6701	Δ*hmgR* + pPL2-*hmgR*	This study
DP-L197	EGD-e	59
DP-L6702	EGD-e Δ*hmgR*	This study
DP-L6703	FSL N1-017 (BEI Resources, NIAID, NIH: *Listeria monocytogenes*, strain FSL N1-017, NR-13231)	47
DP-L6704	FSL N1-017 Δ*hmgR*	This study
DP-L6705	HPB2262 (Aureli 1997)	14
DP-L6706	HPB2262 Δ*hmgR*	This study
DP-L6707	Δ*hmgR* + pPL2-*ispD* (10403S)	This study
DP-L6708	Δ*hmgR* + pPL2-*ispD* (FSL N1-017)	This study
DP-L6709	Δ*hmgR* + pPL2-*ispD* (HPB2262)	This study
DP-L6710	Δ*hmgR* + pPL2-*gcpE* (10403S)	This study
DP-L6711	Δ*hmgR* + pPL2-*gcpE* (FSL N1-017)	This study
DP-L6712	Δ*hmgR* + pPL2-*gcpE* (HPB2262)	This study
DP-L6713	Δ*hmgR* + pPL2-*lytB* (10403S)	This study
DP-L6714	Δ*hmgR* + pPL2-*lytB* (FSL N1-017)	This study
DP-L6715	Δ*hmgR* + pPL2-*lytB* (HPB2262)	This study
DP-L6716	Δ*hmgR* Δ*gcpE*	This study
DP-L6717	Δ*hmgR* Δ*gcpE* + pPL2-*gcpE* (P_{10403S} 10403S)	This study
DP-L6718	Δ*hmgR* Δ*gcpE* + pPL2-*gcpE* (P_{10403S} FSL N1-017)	This study
DP-L6719	Δ*hmgR* Δ*gcpE* + pPL2-*gcpE* (P_{10403S} HPB2262)	This study
DP-L6720	Δ*hmgR* Δ*gcpE* + pPL2-*gcpE* ($10403S^{1-250}$/FSL N1-$017^{251-369}$)	This study
DP-L6721	Δ*hmgR* Δ*gcpE* + pPL2-*gcpE*$^{I343V/D344E}$	This study
DP-L6722	Δ*hmgR* Δ*gcpE* + pPL2-*gcpE*$^{F357Y/V359E}$	This study
DP-L6723	Δ*hmgR* Δ*gcpE* + pPL2-*gcpE*$^{K291T/E293K/V294A}$	This study
DP-L6724	Δ*hmgR* Δ*gcpE* + pPL2-*gcpE*^{K291T}	This study
DP-L6725	Δ*hmgR* Δ*gcpE* + pPL2-*gcpE*^{V294A}	This study
DP-L6726	Δ*hmgR gcpE*$^{K291T/E293K/V294A}$	This study
DP-L2209	*hly*::Tn*917*	26
DP-L6727	*gcpE*$^{K291T/E293K/V294A}$	This study
DP-L6728	*gcpE*$^{K291T/E293K/V294A}$ *hly*::Tn*917*	This study
DP-L6729	Δ*gcpE*	This study
DP-L6730	Δ*gcpE hly*::Tn*917*	This study
DP-L6731	Δ*lytB*	This study
DP-L6732	Δ*lytB hly*::Tn*917*	This study

A large number of clinically significant bacterial and protozoan pathogens, such as *Vibrio cholerae*, *Pseudomonas aeruginosa*, *Clostridium difficile*, *Mycobacterium tuberculosis*, and *Plasmodium* species, have the nonmevalonate pathway and produce HMBPP. However, the nonmevalonate pathway is essential for producing isoprenoid precursors in all of these organisms, making it extremely difficult to separate growth defects from virulence defects. In bacteria that encode both pathways, including *Mycobacterium marinum* (49) and several *Streptomyces* and *Nocardia* species (50), even less is known about isoprenoid pathways. By understanding the role of the nonmevalonate pathway in *L. monocytogenes*, it may be possible to metabolically engineer other bacteria to intentionally manipulate Vγ9Vδ2 T cell activation levels and improve adaptive immune responses to pathogens.

MATERIALS AND METHODS

Construction of *L. monocytogenes* strains. The *L. monocytogenes* strains used in this study are all derived from wild-type 10403S (DP-L6253), unless otherwise noted, and are listed in Table 1. Gene deletions were generated by allelic exchange using the plasmid pKSV7 (51). All *L. monocytogenes* strains were grown in brain heart infusion (BHI) broth supplemented with 5 g/liter yeast extract, 1 g/liter L-cysteine hydrochloride, and 0.001 g/liter resazurin sodium salt, and medium was supplemented with 1 mM mevalonate as needed to support the growth of auxotrophic Δ*hmgR* strains. Mevalonate was produced by hydrolyzing DL-mevalonolactone (CAS number 674-26-0; Sigma-Aldrich) with 1 N NaOH at 37°C for 1 h according to previously reported methods (6). Agar plates were incubated anaerobically using a BD GasPak EZ anaerobic pouch system (no. 260683), and liquid cultures were incubated in an anaerobic chamber (Coy Laboratory Products) with an environment of 2% H_2 balanced with N_2.

TABLE 2 *E. coli* strains

Strain	Plasmid or genotype	Reference or source
XL1-Blue	Cloning; *recA1 endA1 gyrA96 thi-1 hsdR17 supE44 relA1 lac* [F′ *proAB lacI*^{q} *Z*ΔM15 Tn*10* (Tet^{r})]	Stratagene
TOP10	Cloning; F^{-} *mcrA* Δ(*mrr-hsdRMS-mcrBC*) Φ80*lacZ*ΔM15 Δ *lacX74 recA1 araD139* Δ(*araleu*)*7697 galU galK rpsL* (Str^{r}) *endA1 nupG*	Invitrogen
SM10	Conjugation; *thi-1 thr-1 leuB6 tonA21 lacY1 supE44 recA* λ-integrated [RP4-2-Tcr::Mu] *aphA*$^{+}$ (Km^{r}) Tra^{+}	60
DP-E6324	pKSV7-oriT	61
DP-E6733	pKSV7-Δ*hmgR* (10403S/FSL N1-017)	This study
DP-E6734	pKSV7-Δ*hmgR* (EGD-e)	This study
DP-E6735	pKSV7-Δ*hmgR* (HPB2262)	This study
DP-E6736	pKSV7-Δ*gcpE*	This study
DP-E6737	pKSV7-Δ*lytB*	This study
DP-E6738	pKSV7-*gcpE*$^{K291T/E293K/V294A}$	This study
DP-E6333	pPL2t	62
DP-E6739	pPL2-*ispD* (10403S)	This study
DP-E6740	pPL2-*ispD* (FSL N1-017)	This study
DP-E6741	pPL2-*ispD* (HPB2262)	This study
DP-E6742	pPL2-*gcpE* (10403S)	This study
DP-E6743	pPL2-*gcpE* (FSL N1-017)	This study
DP-E6744	pPL2-*gcpE* (HPB2262)	This study
DP-E6745	pPL2-*lytB* (10403S)	This study
DP-E6746	pPL2-*lytB* (FSL N1-017)	This study
DP-E6747	pPL2-*lytB* (HPB2262)	This study
DP-E6748	pPL2-*gcpE* (P_{10403S} FSL N1-017)	This study
DP-E6749	pPL2-*gcpE* (P_{10403S} HPB2262)	This study
DP-E6750	pPL2-*gcpE* (10403S$^{1-250}$/FSL N1-017$^{251-369}$)	This study
DP-E6751	pPL2-*gcpE*$^{I343V/D344E}$	This study
DP-E6752	pPL2-*gcpE*$^{F357Y/V359E}$	This study
DP-E6753	pPL2-*gcpE*$^{K291T/E293K/V294A}$	This study
DP-E6754	pPL2-*gcpE*^{K291T}	This study
DP-E6755	pPL2-*gcpE*^{V294A}	This study
DP-E6756	pPL2-*hmgR*	This study

E. coli strains used in this study are listed in Table 2. For vector construction, plasmids were introduced into TOP10 *E. coli* (Invitrogen) or XL1 Blue *E. coli* (Stratagene). Plasmids were then transformed into SM10 *E. coli* and conjugated into *L. monocytogenes*. PCR was performed with KAPA HiFi DNA polymerase (Kapa Biosystems) or Q5 DNA polymerase (NEB). Positive clones were identified by performing colony PCRs using SapphireAmp fast PCR master mix (TaKaRa Bio) and verified by Sanger sequencing.

Aerobic growth curves. Strains were grown overnight at 37°C in filter-sterilized BHI and were supplemented with 500 μM mevalonate as necessary. Bacteria were washed with phosphate-buffered saline (PBS) and diluted in 20 ml fresh BHI to an optical density at 600 nm (OD_{600}) of 0.01. Cells were cultured at 37°C with shaking, and growth was measured spectrophotometrically hourly.

Anaerobic growth curves. Medium was degassed overnight in an anaerobic chamber to allow residual oxygen to diffuse out of the medium. Overnight cultures of cells were first grown aerobically and were back diluted into anaerobic medium to a concentration of 10^3 CFU/ml. Samples were removed from the chamber daily and plated by 10-fold serial dilutions to enumerate CFU.

Structure prediction. The Phyre2 protein modeling web portal was used to generate a predicted model of *L. monocytogenes* 10403S GcpE (52).

i.v. infections. Intravenous (i.v.) infections were adapted from previously reported methods (53, 54). Briefly, 8-week-old female CD-1 (Charles River) mice were infected i.v. with 10^5 CFU in 200 μl of PBS, and organs were harvested 48 h postinfection. When mice were infected with Δ*hmgR* mutants, the inoculum was increased to 10^6 CFU, and organs were harvested 24 h postinfection due to the growth defect of this strain. To measure organ CFU, mice were euthanized and spleens and livers were removed, homogenized in 5 or 10 ml, respectively, of 0.1% IGEPAL CA-630 (Sigma), and plated to enumerate bacteria.

Oral infections. Oral infections were adapted from previously reported methods (27, 55, 56). Briefly, 5 mg/ml of streptomycin sulfate was added to the drinking water of 8-week-old female CD-1 (Charles River) mice 2 days prior to infection. One day prior to infection, mice were transferred to clean cages and chow was removed to fast the mice overnight. Mice were fed a small piece of white bread inoculated with 10^7 CFU of *L. monocytogenes* in 5 μl of PBS, and 3 μl of butter was overlaid on the bread. When mice were infected with Δ*hmgR* mutants, the inoculum was increased to 10^8 CFU due to the growth defect of this strain. After infection, mice were returned to cages with standard drinking water and chow. To measure infection burden, pellets were collected from each mouse, weighed, homogenized in 1 ml PBS, and plated by serial dilution to enumerate CFU. Homogenates were plated on selective BHI agar supplemented with 6 g/liter lithium chloride, 6 g/liter glycine, 50 mg/liter nalidixic acid, and 200 mg/liter streptomycin (57). Pellets were collected daily for the first 5 days postinfection and every 2 days for the

remainder of the experiment. These studies were carried out in strict accordance with the recommendations in the *Guide for the Care and Use of Laboratory Animals* of the National Institutes of Health (58). All protocols were reviewed and approved by the Animal Care and Use Committee at the University of California, Berkeley (AUP-2016-05-8811).

SUPPLEMENTAL MATERIAL

Supplemental material is available online only.

SUPPLEMENTAL FILE 1, PDF file, 2.4 MB.

SUPPLEMENTAL FILE 2, PDF file, 0.02 MB.

ACKNOWLEDGMENTS

We thank J. D. Keasling and J. Kirby for suggesting we examine our mutant anaerobically. We also thank S. H. Light and A. Louie for critical reading of the manuscript and S. H. Light for help with structure modeling.

This work was supported by the National Institutes of Health grants 1P01 AI063302 (D.A.P.) and 1R01 AI027655 (D.A.P.).

REFERENCES

1. Lombard J, Moreira D. 2011. Origins and early evolution of the mevalonate pathway of isoprenoid biosynthesis in the three domains of life. Mol Biol Evol 28:87–99. https://doi.org/10.1093/molbev/msq177.
2. Rohmer M. 2008. From molecular fossils of bacterial hopanoids to the formation of isoprene units: discovery and elucidation of the methylerythritol phosphate pathway. Lipids 43:1095–1107. https://doi.org/10.1007/s11745-008-3261-7.
3. Kuzuyama T, Seto H. 2012. Two distinct pathways for essential metabolic precursors for isoprenoid biosynthesis. Proc Jpn Acad Ser B Phys Biol Sci 88:41–52. https://doi.org/10.2183/pjab.88.41.
4. Ahyong V, Berdan CA, Nomura DK, Welch MD. 2019. A metabolic dependency for host isoprenoids in the obligate intracellular pathogen *Rickettsia parkeri* underlies a sensitivity for the statin class of host-targeted therapeutics. mSphere 4:e00536-19. https://doi.org/10.1128/mSphere.00536-19.
5. Heuston S, Begley M, Gahan CGM, Hill C. 2012. Isoprenoid biosynthesis in bacterial pathogens. Microbiology 158:1389–1401. https://doi.org/10.1099/mic.0.051599-0.
6. Begley M, Bron PA, Heuston S, Casey PG, Englert N, Wiesner J, Jomaa H, Gahan CGM, Hill C. 2008. Analysis of the isoprenoid biosynthesis pathways in *Listeria monocytogenes* reveals a role for the alternative 2-C-methyl-D-erythritol 4-phosphate pathway in murine infection. Infect Immun 76:5392–5401. https://doi.org/10.1128/IAI.01376-07.
7. Heuston S, Begley M, Davey MS, Eberl M, Casey PG, Hill C, Gahan C. 2012. HmgR, a key enzyme in the mevalonate pathway for isoprenoid biosynthesis, is essential for growth of *Listeria monocytogenes* EGDe. Microbiology 158:1684–1693. https://doi.org/10.1099/mic.0.056069-0.
8. Boutin L, Scotet E. 2018. Towards deciphering the hidden mechanisms that contribute to the antigenic activation process of human Vγ9Vδ2 T cells. Front Immunol 9:828. https://doi.org/10.3389/fimmu.2018.00828.
9. Gu S, Nawrocka W, Adams EJ. 2015. Sensing of pyrophosphate metabolites by Vγ9Vδ2 T cells. Front Immunol 6:668. https://doi.org/10.3389/fimmu.2014.00688.
10. Tyler CJ, Doherty DG, Moser B, Eberl M. 2015. Human Vγ9/Vδ2 T cells: innate adaptors of the immune system. Cell Immunol 296:10–21. https://doi.org/10.1016/j.cellimm.2015.01.008.
11. Willcox BE, Willcox CR. 2019. γδ TCR ligands: the quest to solve a 500-million-year-old mystery. Nat Immunol 20:121–128. https://doi.org/10.1038/s41590-018-0304-y.
12. Flickinger J, Rodeck U, Snook A. 2018. *Listeria monocytogenes* as a vector for cancer immunotherapy: current understanding and progress. Vaccines 6:48. https://doi.org/10.3390/vaccines6030048.
13. den Bakker HC, Desjardins CA, Griggs AD, Peters JE, Zeng Q, Young SK, Kodira CD, Yandava C, Hepburn TA, Haas BJ, Birren BW, Wiedmann M. 2013. Evolutionary dynamics of the accessory genome of *Listeria monocytogenes*. PLoS One 8:e67511. https://doi.org/10.1371/journal.pone.0067511.
14. Aureli P, Fiorucci GC, Caroli D, Marchiaro G, Novara O, Leone L, Salmaso S. 2000. An outbreak of febrile gastroenteritis associated with corn contaminated by *Listeria monocytogenes*. N Engl J Med 342:1236–1241. https://doi.org/10.1056/NEJM200004273421702.
15. Maury MM, Tsai YH, Charlier C, Touchon M, Chenal-Francisque V, Leclercq A, Criscuolo A, Gaultier C, Roussel S, Brisabois A, Disson O, Rocha EPC, Brisse S, Lecuit M. 2016. Uncovering *Listeria monocytogenes* hypervirulence by harnessing its biodiversity. Nat Genet 48:308–313. https://doi.org/10.1038/ng.3501.
16. Adam P, Hecht S, Eisenreich W, Kaiser J, Grawert T, Arigoni D, Bacher A, Rohdich F. 2002. Biosynthesis of terpenes: studies on 1-hydroxy-2-methyl-2-(E)-butenyl 4-diphosphate reductase. Proc Natl Acad Sci U S A 99:12108–12113. https://doi.org/10.1073/pnas.182412599.
17. Wolff M, Seemann M, Grosdemange-Billiard C, Tritsch D, Campos N, Rodríguez-Concepción M, Boronat A, Rohmer M. 2002. Isoprenoid biosynthesis via the methylerythritol phosphate pathway. (E)-4-Hydroxy-3-methylbut-2-enyl diphosphate: chemical synthesis and formation from methylerythritol cyclodiphosphate by a cell-free system from *Escherichia coli*. Tetrahedron Lett 43:2555–2559. https://doi.org/10.1016/S0040-4039(02)00293-9.
18. Flint DH, Tuminello JF, Emptage MH. 1993. The inactivation of Fe-S cluster containing hydro-lyases by superoxide. J Biol Chem 268:22369–22376.
19. Rivasseau C, Seemann M, Boisson A-M, Streb P, Gout E, Douce R, Rohmer M, Bligny R. 2009. Accumulation of 2-C-methyl-D-erythritol 2,4-cyclodiphosphate in illuminated plant leaves at supraoptimal temperatures reveals a bottleneck of the prokaryotic methylerythritol 4-phosphate pathway of isoprenoid biosynthesis. Plant Cell Environ 32:82–92. https://doi.org/10.1111/j.1365-3040.2008.01903.x.
20. Artsatbanov VY, Vostroknutova GN, Shleeva MO, Goncharenko AV, Zinin AI, Ostrovsky DN, Kapreliants AS. 2012. Influence of oxidative and nitrosative stress on accumulation of diphosphate intermediates of the non-mevalonate pathway of isoprenoid biosynthesis in corynebacteria and mycobacteria. Biochemistry 77:362–371. https://doi.org/10.1134/S0006297912040074.
21. Martien JI, Hebert AS, Stevenson DM, Regner MR, Khana DB, Coon JJ, Amador-Noguez D. 2019. Systems-level analysis of oxygen exposure in *Zymomonas mobilis*: implications for isoprenoid production. mSystems 4:e00284-18. https://doi.org/10.1128/mSystems.00284-18.
22. Begley M, Gahan CGM, Kollas AK, Hintz M, Hill C, Jomaa H, Eberl M. 2004. The interplay between classical and alternative isoprenoid biosynthesis controls γδ T cell bioactivity of *Listeria monocytogenes*. FEBS Lett 561:99–104. https://doi.org/10.1016/S0014-5793(04)00131-0.
23. Hardy J, Margolis JJ, Contag CH. 2006. Induced biliary excretion of *Listeria monocytogenes*. Infect Immun 74:1819–1827. https://doi.org/10.1128/IAI.74.3.1819-1827.2006.
24. Melton-Witt JA, Rafelski SM, Portnoy DA, Bakardjiev AI. 2012. Oral infection with signature-tagged *Listeria monocytogenes* reveals organ-specific growth and dissemination routes in guinea pigs. Infect Immun 80:720–732. https://doi.org/10.1128/IAI.05958-11.
25. Zhang T, Abel S, Abel Zur Wiesch P, Sasabe J, Davis BM, Higgins DE, Waldor MK. 2017. Deciphering the landscape of host barriers to *Listeria monocytogenes* infection. Proc Natl Acad Sci U S A 114:6334–6339. https://doi.org/10.1073/pnas.1702077114.
26. Camilli A, Portnoy DA, Youngman P. 1990. Insertional mutagenesis of

Listeria monocytogenes with a novel Tn*917* derivative that allows direct cloning of DNA flanking transposon insertions. J Bacteriol 172:3738–3744. https://doi.org/10.1128/jb.172.7.3738-3744.1990.
27. Becattini S, Littmann ER, Carter RA, Kim SG, Morjaria SM, Ling L, Gyaltshen Y, Fontana E, Taur Y, Leiner IM, Pamer EG. 2017. Commensal microbes provide first line defense against *Listeria monocytogenes* infection. J Exp Med 214:1973–1989. https://doi.org/10.1084/jem.20170495.
28. Müller-Herbst S, Wüstner S, Mühlig A, Eder D, M Fuchs T, Held C, Ehrenreich A, Scherer S, Fuchs TM, Held C, Ehrenreich A, Scherer S. 2014. Identification of genes essential for anaerobic growth of *Listeria monocytogenes*. Microbiology 160:752–765. https://doi.org/10.1099/mic.0.075242-0.
29. Romick TL, Fleming HP, McFeeters RF. 1996. Aerobic and anaerobic metabolism of *Listeria monocytogenes* in defined glucose medium. Appl Environ Microbiol 62:304–307.
30. Imlay JA. 2006. Iron-sulphur clusters and the problem with oxygen. Mol Microbiol 59:1073–1082. https://doi.org/10.1111/j.1365-2958.2006.05028.x.
31. Johnson DC, Dean DR, Smith AD, Johnson MK. 2005. Structure, function, and formation of biological iron-sulfur clusters. Annu Rev Biochem 74:247–281. https://doi.org/10.1146/annurev.biochem.74.082803.133518.
32. Jang S, Imlay JA. 2010. Hydrogen peroxide inactivates the *Escherichia coli* Isc iron-sulphur assembly system, and OxyR induces the Suf system to compensate. Mol Microbiol 78:1448–1467. https://doi.org/10.1111/j.1365-2958.2010.07418.x.
33. Outten FW, Djaman O, Storz G. 2004. A suf operon requirement for Fe-S cluster assembly during iron starvation in *Escherichia coli*. Mol Microbiol 52:861–872. https://doi.org/10.1111/j.1365-2958.2004.04025.x.
34. Tanaka N, Kanazawa M, Tonosaki K, Yokoyama N, Kuzuyama T, Takahashi Y. 2016. Novel features of the ISC machinery revealed by characterization of *Escherichia coli* mutants that survive without iron-sulfur clusters. Mol Microbiol 99:835–848. https://doi.org/10.1111/mmi.13271.
35. Yokoyama N, Nonaka C, Ohashi Y, Shioda M, Terahata T, Chen W, Sakamoto K, Maruyama C, Saito T, Yuda E, Tanaka N, Fujishiro T, Kuzuyama T, Asai K, Takahashi Y. 2018. Distinct roles for U-type proteins in iron–sulfur cluster biosynthesis revealed by genetic analysis of the *Bacillus subtilis sufCDSUB* operon. Mol Microbiol 107:688–703. https://doi.org/10.1111/mmi.13907.
36. Lee M, Gräwert T, Quitterer F, Rohdich F, Eppinger J, Eisenreich W, Bacher A, Groll M. 2010. Biosynthesis of isoprenoids: crystal structure of the [4Fe-4S] cluster protein IspG. J Mol Biol 404:600–610. https://doi.org/10.1016/j.jmb.2010.09.050.
37. Quitterer F, Frank A, Wang K, Rao G, O'Dowd B, Li J, Guerra F, Abdel-Azeim S, Bacher A, Eppinger J, Oldfield E, Groll M. 2015. Atomic-resolution structures of discrete stages on the reaction coordinate of the [Fe4S4] enzyme IspG (GcpE). J Mol Biol 427:2220–2228. https://doi.org/10.1016/j.jmb.2015.04.002.
38. Rekittke I, Jomaa H, Ermler U. 2012. Structure of the GcpE (IspG)-MEcPP complex from *Thermus thermophilus*. FEBS Lett 586:3452–3457. https://doi.org/10.1016/j.febslet.2012.07.070.
39. Rekittke I, Nonaka T, Wiesner J, Demmer U, Warkentin E, Jomaa H, Ermler U. 2011. Structure of the E-1-hydroxy-2-methyl-but-2-enyl-4-diphosphate synthase (GcpE) from *Thermus thermophilus*. FEBS Lett 585:447–451. https://doi.org/10.1016/j.febslet.2010.12.012.
40. Zhao L, Chang W-C, Xiao Y, Liu H-W, Liu P. 2013. Methylerythritol phosphate pathway of isoprenoid biosynthesis. Annu Rev Biochem 82:497–530. https://doi.org/10.1146/annurev-biochem-052010-100934.
41. Qiu J, Yan L, Chen J, Chen CY, Shen L, Letvin NL, Haynes BF, Freitag N, Rong L, Frencher JT, Huang D, Wang X, Chen ZW. 2011. Intranasal vaccination with the recombinant *Listeria monocytogenes* Δ*actA prfA** mutant elicits robust systemic and pulmonary cellular responses and secretory mucosal IgA. Clin Vaccine Immunol 18:640–646. https://doi.org/10.1128/CVI.00254-10.
42. Ryan-Payseur B, Frencher J, Shen L, Chen CY, Huang D, Chen ZW. 2012. Multieffector-functional immune responses of HMBPP-specific Vγ2Vδ2 T cells in nonhuman primates inoculated with *Listeria monocytogenes* Δ*actA prfA**. J Immunol 189:1285–1293. https://doi.org/10.4049/jimmunol.1200641.
43. Frencher JT, Shen H, Yan L, Wilson JO, Freitag NE, Rizzo N, Chen CY, Chen ZW, Rizzo AN, Chen CY, Chen ZW. 2014. HMBPP-deficient *Listeria* mutant immunization alters pulmonary/systemic responses, effector functions, and memory polarization of Vγ2Vδ2 T cells. J Leukoc Biol 96:957–967. https://doi.org/10.1189/jlb.6HI1213-632R.
44. Shen H, Wang Y, Chen CY, Frencher J, Huang D, Yang E, Ryan-Payseur B, Chen ZW. 2015. Th17-related cytokines contribute to recall-like expansion/effector function of HMBPP-specific Vγ2Vδ2 T cells after *Mycobacterium tuberculosis* infection or vaccination. Eur J Immunol 45:442–451. https://doi.org/10.1002/eji.201444635.
45. Shen L, Frencher J, Huang D, Wang W, Yang E, Chen CY, Zhang Z, Wang R, Qaqish A, Larsen MH, Shen H, Porcelli SA, Jacobs WR, Chen ZW. 2019. Immunization of Vγ2Vδ2 T cells programs sustained effector memory responses that control tuberculosis in nonhuman primates. Proc Natl Acad Sci U S A 116:6371–6378. https://doi.org/10.1073/pnas.1811380116.
46. Hoeres T, Smetak M, Pretscher D, Wilhelm M. 2018. Improving the efficiency of Vγ9Vδ2 T-cell immunotherapy in cancer. Front Immunol 9:800. https://doi.org/10.3389/fimmu.2018.00800.
47. Gray MJ, Zadoks RN, Fortes ED, Dogan B, Cai S, Chen Y, Scott VN, Gombas DE, Boor KJ, Wiedmann M. 2004. *Listeria monocytogenes* isolates from foods and humans form distinct but overlapping populations. Appl Environ Microbiol 70:5833–5841. https://doi.org/10.1128/AEM.70.10.5833-5841.2004.
48. McCarthy NE, Eberl M. 2018. Human γδ T-cell control of mucosal immunity and inflammation. Front Immunol 9:985. https://doi.org/10.3389/fimmu.2018.00985.
49. Stinear TP, Seemann T, Harrison PF, Jenkin GA, Davies JK, Johnson PD, Abdellah Z, Arrowsmith C, Chillingworth T, Churcher C, Clarke K, Cronin A, Davis P, Goodhead I, Holroyd N, Jagels K, Lord A, Moule S, Mungall K, Norbertczak H, Quail MA, Rabbinowitsch E, Walker D, White B, Whitehead S, Small PL, Brosch R, Ramakrishnan L, Fischbach MA, Parkhill J, Cole ST. 2008. Insights from the complete genome sequence of *Mycobacterium marinum* on the evolution of *Mycobacterium tuberculosis*. Genome Res 18:729–741. https://doi.org/10.1101/gr.075069.107.
50. Dairi T. 2005. Studies on biosynthetic genes and enzymes of isoprenoids produced by actinomycetes. Jpn J Antibiot 58:87–98.
51. Smith K, Youngman P. 1992. Use of a new integrational vector to investigate compartment-specific expression of the *Bacillus subtilis spollM* gene. Biochimie 74:705–711. https://doi.org/10.1016/0300-9084(92)90143-3.
52. Kelley LA, Mezulis S, Yates CM, Wass MN, Sternberg M. 2015. The Phyre2 web portal for protein modeling, prediction and analysis. Nat Protoc 10:845–858. https://doi.org/10.1038/nprot.2015.053.
53. Portman JL, Dubensky SB, Peterson BN, Whiteley AT, Portnoy DA. 2017. Activation of the *Listeria monocytogenes* virulence program by a reducing environment. mBio 8:e01595-17. https://doi.org/10.1128/mBio.01595-17.
54. Auerbuch V, Lenz LL, Portnoy DA. 2001. Development of a competitive index assay to evaluate the virulence of *Listeria monocytogenes actA* mutants during primary and secondary infection of mice. Infect Immun 69:5953–5957. https://doi.org/10.1128/iai.69.9.5953-5957.2001.
55. Bou Ghanem EN, Jones GS, Myers-Morales T, Patil PD, Hidayatullah AN, D'Orazio SEF. 2012. InlA promotes dissemination of *Listeria monocytogenes* to the mesenteric lymph nodes during food borne infection of mice. PLoS Pathog 8:e1003015. https://doi.org/10.1371/journal.ppat.1003015.
56. Light SH, Su L, Rivera-Lugo R, Cornejo JA, Louie A, Iavarone AT, Ajo-Franklin CM, Portnoy DA. 2018. A flavin-based extracellular electron transfer mechanism in diverse Gram-positive bacteria. Nature 562:140–144. https://doi.org/10.1038/s41586-018-0498-z.
57. Lachica RV. 1990. Selective plating medium for quantitative recovery of food-borne *Listeria monocytogenes*. Appl Environ Microbiol 56:167–169.
58. National Research Council. 2011. Guide for the care and use of laboratory animals, 8th ed. National Academies Press, Washington, DC.
59. Bécavin C, Bouchier C, Lechat P, Archambaud C, Creno S, Gouin E, Wu Z, Kühbacher A, Brisse S, Pucciarelli MG, García-del Portillo F, Hain T, Portnoy DA, Chakraborty T, Lecuit M, Pizarro-Cerdá J, Moszer I, Bierne H, Cossart P. 2014. Comparison of widely used *Listeria monocytogenes* strains EGD, 10403S, and EGD-e highlights genomic variations underlying differences in pathogenicity. mBio 5:e00969-14. https://doi.org/10.1128/mBio.00969-14.
60. Simon R, Priefer U, Pühler A. 1983. A broad host range mobilization system for in vivo genetic engineering: transposon mutagenesis in Gram negative bacteria. Nat Biotechnol 1:784–791. https://doi.org/10.1038/nbt1183-784.
61. Camilli A, Tilney LG, Portnoy DA. 1993. Dual roles of *plcA* in *Listeria monocytogenes* pathogenesis. Mol Microbiol 8:143–157. https://doi.org/10.1111/j.1365-2958.1993.tb01211.x.
62. Whiteley AT, Pollock AJ, Portnoy DA, Whiteley AT, Pollock AJ, Portnoy DA. 2015. The PAMP c-di-AMP is essential for *Listeria monocytogenes* growth in rich but not minimal media due to a toxic increase in (p)ppGpp. Cell Host Microbe 17:788–798. https://doi.org/10.1016/j.chom.2015.05.006.